Optimising Buoy Design for Wave Energy Harvesting using the WITT Device

Gabriel Cairns [1]†, Nicholas Ryan [1], John Paul Alexander [2], Graeme Hocking [3], Brady Metherall [1], Bernard Piette [4], Niall Rodgers [5], Sangeetha Sampath [6], and Robert J. Whittaker [7]

[1] *University of Oxford, UK*
[2] *University of Manchester, UK*
[3] *Murdoch University, Australia*
[4] *University of Durham, UK*
[5] *University of Birmingham, UK*
[6] *University of Bath, UK*
[7] *University of East Anglia, UK*

(*Communicated to* MIIR *on 24 July 2024*)

Study Group: 180th European Study Group with Industry, 24th–29th June 2024, University of Birmingham, UK

Communicated by: Rosemary Dyson and James Andrews, University of Birmingham

Industrial Partner: WITT Energy (www.witt-energy.com/)

Presenter: Mairi Wickett, Martin Wickett

Team Members: Paul Alexander, University of Manchester; Gabriel Cairns, University of Oxford; Daniel Herring, University of Birmingham; Graeme Hocking, Murdoch University; Andrew Lacey, Heriot-Watt University; Robert Leek, University of Birmingham; David Leppinen, University of Birmingham; Galane Luo, University of Birmingham; Brady Metherall, University of Oxford; Gavin Moreton, University of Leicester; John Ockendon, University of Oxford; Jeremy Parker, University of Dundee; Bernard Piette, University of Durham; Richard Purvis, University of East Anglia; Niall Rodgers, University of Birmingham; Nicholas Ryan, University of Oxford; Sangeetha Sampath, University of Bath; Tony Samuel, University of Birmingham and University of Exeter; Robert Whittaker, University of East Anglia.

Industrial Sector: Energy/Utilities

Key Words: Buoy; Lagrangian mechanics; Ocean dynamics; Wave energy

MSC2020 Codes: 70E99, 70K30, 70K40

† Corresponding Author: `cairns@maths.ox.ac.uk`

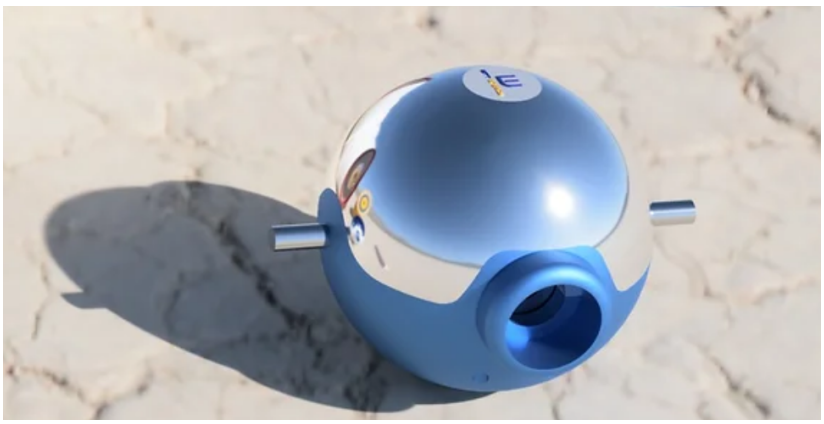

Figure 1. The WITT device.

Summary

This work considers the design of a wave energy converter employing the WITT device: a machine that is able to convert motion in all 6 degrees of freedom into electrical power. Various designs for housing the WITT device inside a buoy are investigated with the aim of converting the forcing from low-frequency ocean waves to a higher-frequency motion at which the WITT generates power most effectively. By modelling the rigid-body motion of a buoy in response to a provided ocean wave forcing and the dynamics of the internal mechanisms within the buoy, we explore how nonlinear oscillation dynamics may achieve the desired frequency amplification.

1 Introduction

The WITT ("Whatever Input to Torsion Transfer") is a unique device that converts oscillations in all 6 degrees of freedom (translation and rotation in 3 dimensions) into electrical power through the use of a pendulum and gearbox mechanism. Such a device may be employed as a wave energy converter [6], enabling the ongoing generation of energy at sea, to be used for example, to power offshore sensors and monitoring devices. This is achieved by mounting the WITT within a buoy.

Previous experimental results [2] found that the WITT produces power most effectively when excited at or above its resonant frequency of 1.2 Hz. This frequency is several times higher than typical frequencies associated with the power spectrum of ocean waves, meaning that frequency amplification is required in order for the WITT to convert wave energy effectively. Previous modelling has considered the use of counterweights or a system of springs in order to achieve this desired frequency amplification [2, 6], or the placement of the WITT underwater to utilise vortex-induced vibrations [3, 16]. Our research further considers the means by which buoy design may be optimised in order to achieve the effective conversion of wave energy by the WITT.

The goal of our modelling is to design a mechanism by which the lower-frequency forc-

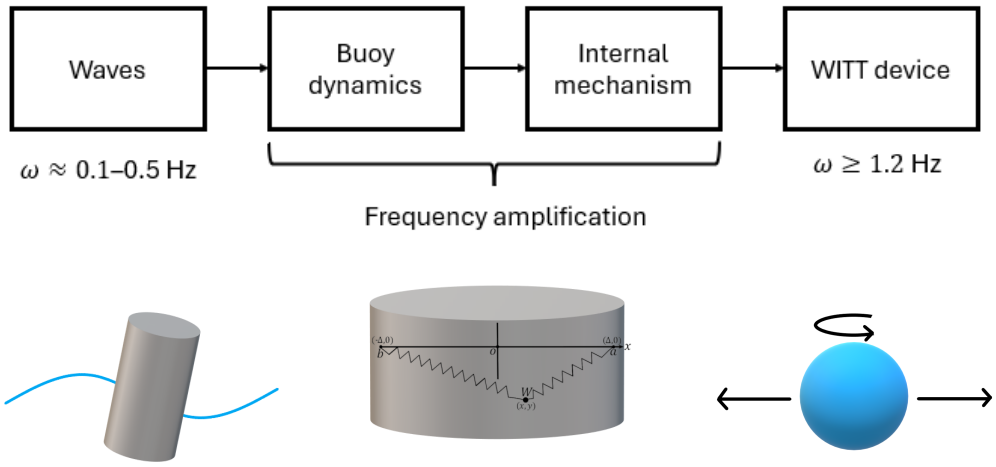

Figure 2. Flowchart of modelling approach.

ing associated with ocean waves may be translated into the higher-frequency oscillations required for the WITT device to function effectively. We aim to achieve this frequency amplification through the design of the buoy in which the WITT device is embedded. This could be achieved through designing a buoy of a certain shape that will respond nonlinearly to forcing by ocean waves, or through some internal mechanism that the WITT device is moved about within the buoy.

Our modelling approach therefore breaks into several distinct levels, shown in Figure 2. Firstly, we require a realistic parameterisation of the frequency, amplitude, and wavelength of ocean waves. This is then used to force a model of rigid-body buoy motion that determines the vertical and angular displacement experienced by the buoy. If the frequency amplification achieved at this stage is insufficient, an internal mechanism within the buoy must be forced according this motion. Finally, this mechanism imparts some motion to the WITT device itself. The mechanism by which WITT device converts motion into power has been modelled previously [2, 3, 6], and we regard this stage as a solved problem.

A more complete model should also incorporate feedback from an internal mechanism onto the rigid-body motion of the buoy. However, in this study we ignore these effects for simplicity.

2 Modelling waves in the ocean

Ultimately, our model requires a mathematical description of waves in the ocean for a typical use case of the WITT device as an input. An exact parameterisation of ocean waves across the use cases of the WITT is impossible because the dynamics depend on many things, such as weather conditions and ocean depth. Nevertheless, we need some characterisation of the motion of the ocean surface, including the tilt, and its horizontal and vertical displacement. To achieve this, we combine linear wave theory with observational surface height data from the Pacific ocean [8].

2.1 Linear free-surface wave theory

There is a standard theory describing linearised free-surface gravity waves on an ocean of uniform finite depth and infinite horizontal extent (see, for example, [12]). Upon making the assumption that the wave height is small compared with both the wavelength and ocean depth, the solution for the free surface perturbation in one dimensions is a superposition of harmonic waves of the form

$$\zeta(x,t) = \int_0^\infty A(k)\sin(kx - \omega t)\,\mathrm{d}k\,, \tag{2.1}$$

where x is a horizontal coordinate, t is time, A is the (vertical) wave amplitude, k is the wavenumber and ω is the angular frequency. The dispersion relation, linking the frequency and wavenumber, is given by

$$\omega^2 = gk\tanh(kD)\,, \tag{2.2}$$

where D is the depth of the ocean and g is the acceleration due to gravity. For a given wavenumber, the vertical motion has amplitude $A(k)$, while the horizontal motion has amplitude $A(k)\coth(kD)$. The gradient of the free surface is given by $\partial\zeta/\partial x$, and so has amplitude $A(k)k$.

There are two limiting cases. If $kD \gg 1$, then $\tanh(kD) \sim 1$ and the dispersion relation becomes

$$\omega^2 = gk\,. \tag{2.3}$$

This is known as the deep-water limit. In this case, the fluid parcels oscillate in a circular motion, with equal horizontal and vertical amplitudes. Conversely, if $kD \ll 1$ (i.e., the wavelength is much larger than the ocean depth), then $\tanh(kD) \sim kD$ and the dispersion relation becomes

$$\omega^2 = gDk^2\,. \tag{2.4}$$

This is known as the shallow-water limit. In this case, the fluid particles oscillate following elliptical paths with a larger horizontal displacement than vertical. It is common to describe ocean waves using the (non-angular) frequency $\nu = 2\pi\omega$, wavelength $\lambda = k/2\pi$, and wave height $H = 2A$.

Given a frequency ω (or ν) and ocean depth D, to solve for the wavenumber k (or wavelength λ), we can write $\kappa = kD$, and then rearrange (2.2) to give

$$\kappa\tanh\kappa = \frac{\omega^2 D}{g}\,. \tag{2.5}$$

If $\omega^2 D/g$ is large, then (2.5) gives that κ must be large, which puts us in the deep-water limit, meaning we can make use of the approximation (2.3). If $\omega^2 D/g$ is small, then κ must be small. Hence, we are in the shallow-water limit and can make use of the approximation (2.4). If neither case applies, then we must solve the full transcendental equation (2.5) for κ in order to recover the wavenumber k.

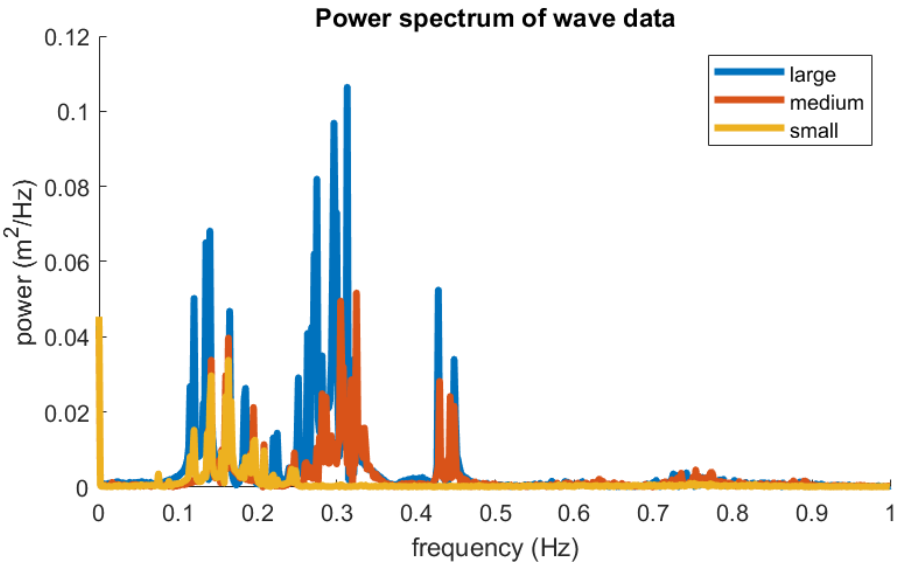

Figure 3. Power spectrum of buoy data, showing the frequency of vertical oscillations under large, medium and small amplitude waves.

2.2 Ocean wave data

Using vertical displacement data [8] measured from a buoy in the Pacific for large, medium, and small amplitude waves at 0.1 second intervals for a 10-minute duration, we use the discrete Fourier transform to determine the peak frequencies of ocean forcing along with the corresponding amplitudes. The power spectrum is shown in Figure 3. We find peaks around 0.15, 0.3, and 0.45 Hz. Therefore, we approximate this forcing as the sum of three sinusoids.

From this data, we wish to compute representative frequencies and amplitudes of the vertical and tilt motion of the ocean surface. With a typical offshore ocean depth of $D \approx 100$ m we have

$$\frac{\omega^2 D}{g} = \frac{(2\pi\nu)^2 D}{g} \approx 35\,, \tag{2.6}$$

which we consider large, and thus we are in the deep-water limit. For open ocean, the value of D would be larger and the same limit would apply. This means that dispersion relation can be approximated by (2.3), hence the wavenumber is

$$k = \frac{\omega^2}{g} = \frac{(2\pi\nu)^2}{g} \approx 0.36 \text{ m}^{-1}\,, \tag{2.7}$$

and then the wavelength is

$$\lambda = \frac{2\pi}{k} \approx 18 \text{ m}\,. \tag{2.8}$$

The amplitudes of the horizontal and vertical motion of the fluid particles on the free surface are both $A \approx 1$ m [8]. The amplitude of the oscillation in the gradient of the surface is $Ak \approx 0.36$. This gives the amplitude in the oscillation in the angle of the

surface as

$$\sigma_{\max} = \tan^{-1}(Ak) \approx 0.35\,. \tag{2.9}$$

We note that the possible use cases of the WITT are in theory highly diverse, so that the above values represent a particular case under fairly typical conditions. However, there is scope for a buoy to be deployed in a range of weather conditions, which would produce different wave amplitudes A.

3 Nonlinear oscillators to produce frequency escalation

The fundamental issue in this project is to take the natural frequency of the waves in the local environment, whether that be a lake, a bay, or open ocean, and design a system that will excite oscillations at a higher frequency than the forcing frequency. It is well known that in a linear system, the response will ultimately be at the same frequency as the input. In order to produce a higher frequency output than a the natural input frequency requires a nonlinearity in the system.

A classical nonlinear equation that can demonstrate this capacity is the so-called "Duffing's equation" [7]. One mechanical system that produces a response described by this equation is that studied by Duffing himself, but it is also seen in several different mechanical spring-mass systems and in the oscillations of a long beam. In the "Duffing Oscillator" [7], the restoring force is proportional to the cube of the displacement, $x(t)$, resulting in the equation

$$\frac{\mathrm{d}^2x}{\mathrm{d}t^2} + 2\gamma\frac{\mathrm{d}x}{\mathrm{d}t} + \omega_0^2 x + \eta x^3 = F\cos\omega t, \tag{3.1}$$

where γ is the coefficient of damping, ω_0 is the natural frequency of the equivalent linear system, *i.e.* that with $\eta = 0$ and $F = 0$, η is the coefficient of the nonlinear restoring force, and F is the amplitude of the forcing. There is a vast literature discussing the many aspects and behaviour of such systems, see for example [1, 11].

The most important feature of this work is the frequency response of the system for different values of forcing. Figure 4 shows a numerical solution to (3.1) with a response that becomes periodic (solid lines) after some initial transients, with clearly higher frequency oscillations occurring than the original forcing (dashed line). Also indicated is the power spectrum indicating the response at different frequencies. The leftmost spike is that for the frequency of the forcing, and there are clearly responses at higher values close to the harmonics of the natural frequency. At some values of the parameters the response is chaotic, but importantly the frequency response retains a similar escalation, albeit slightly spread out.

The frequency response of the system for any set of parameters can be obtained by assuming a solution for the displacement, $x(t)$ of the form

$$x(t) = A(\omega)\cos(\omega t), \tag{3.2}$$

and then determining the amplitude of each frequency in the Fourier decomposition. Full

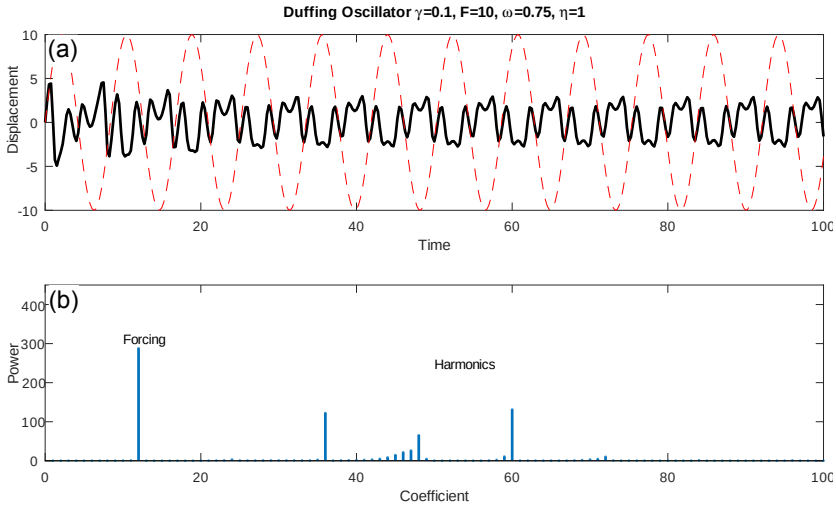

Figure 4. Displacement and power spectrum for a simulation of the Duffing equation (3.1) with $\gamma = 0.1$, $F = 10$, and $\omega = 0.75$. In (a) the solid lines are the displacement and the dashed line is the original forcing function.

details can be found in [11] and the resulting approximate frequency response is given by

$$\left[\left(\omega^2 - \omega_0^2 - \frac{3}{4}\eta A(\omega)^2\right)^2 + (2\gamma\omega)^2\right] A(\omega)^2 = F^2. \tag{3.3}$$

It is notable that this function is multiple-valued for many values of the parameters and hence it is possible to produce a multi-frequency response. Substituting values for the parameters for a particular system will provide the amplitude of the response of each forcing frequency.

Therefore, insights from this model can be used for designing an appropriate system within the WITT device. How this system or one with similar properties can be designed in practice is the subject of the remainder of this report.

4 Buoy dynamics in sea water

Before considering the design of an internal nonlinear oscillator, we must first determine the response of the buoy as a whole to ocean wave forcing. The resulting motion may then be used to force a model of internal buoy dynamics. We assume a homogeneous, cylindrical buoy, having mass M, height L, diameter W, and base area S. We take z to be the depth of the centre of mass in the water. Then, at rest, we have

$$M\,g = \rho_w S(d + z), \tag{4.1}$$

where $d = L/2$, ρ_w is the density of water, and g is gravity. When the buoy is tilted by an angle, the volume of the buoy under water remains $S(d + z)$. This can be shown

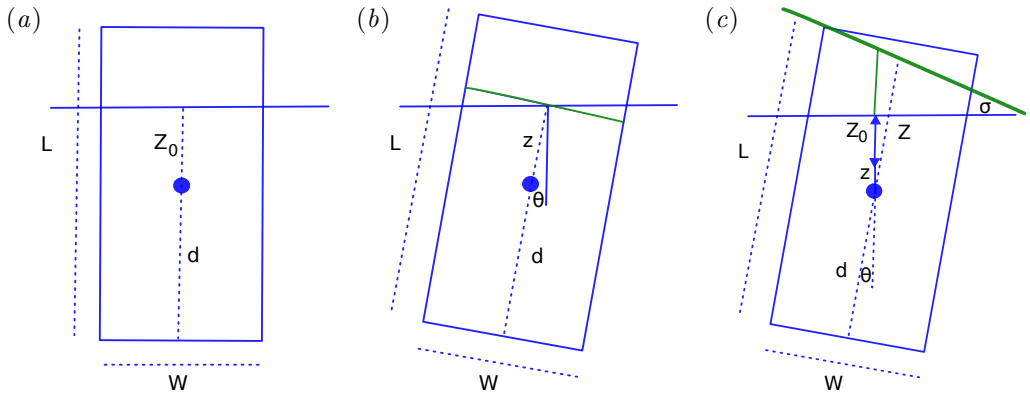

Figure 5. Parametrisation of a buoy. (a) buoy at rest, (b) rotated buoy, (c) rotated buoy under a wave.

graphically by noticing in Figure 5b that the volume under water above the green line can be "moved" to the area above the water on the left, restoring the original profile of the buoy.

To compute the dynamical equation, we use the Lagrangian formalism. Sea waves will move the buoy vertically by an amount A, and the sea surface will be at an angle σ to the horizontal. The "plunging" distance between the water surface and the centre of the buoy is

$$Z = A - z + Z_0, \tag{4.2}$$

where

$$Z_0 = \frac{M\,g}{S} - \frac{L}{2} \tag{4.3}$$

is the "plunging" distance at rest. The potential energy of the buoy is then

$$V = M\,g\,z - \frac{1}{2} g \rho_w S (d+Z)^2 + \frac{k_w}{2}(\theta - \sigma)^2. \tag{4.4}$$

The second term corresponds to the potential energy needed to submerge the buoy in water. In addition, we add the third term to couple the tilting of the buoy, given by θ, with the slope of the water surface. For a cylindrical buoy, the angle between the water surface is not affected by how much it is immersed in water, but for other shapes it generally will be. This third term is a Hooke's law style potential with 'spring constant' k_w.

The kinetic energy of the buoy is

$$T = \frac{M}{2}\left(\frac{\mathrm{d}z}{\mathrm{d}t}\right)^2 + \frac{J}{2}\left(\frac{\mathrm{d}\theta}{\mathrm{d}t}\right)^2, \tag{4.5}$$

where J is the moment of inertia of the buoy around the horizontal axis going through its centre of mass. For a homogeneous cylinder of radius r, we have

$$\begin{aligned} J(L,r) &= \frac{1}{4} M r^2 + \frac{1}{3}\,M\,L^2 \\ &= \pi\rho\left(\frac{1}{4}\,L\,r^4 + \frac{1}{3}\,L^3\,r^2\right), \end{aligned} \tag{4.6}$$

where ρ is density. For a hollow cylinder of thickness ϵ, we have

$$J_{hc} = J(L, r) - J(L - \epsilon, r - \epsilon). \tag{4.7}$$

The Lagrangian is given by

$$\mathcal{L} = T - V. \tag{4.8}$$

Guided by §2.2, we assume that the incoming ocean waves are of the form

$$A(t, x) = \sum_i a_i \sin\left(2\pi\left(\nu_i t - \frac{x}{\lambda_i}\right) + \phi_i\right). \tag{4.9}$$

Then

$$\sigma(t, x) = -\sum_i \tan^{-1}\left(\frac{2\pi a_i}{\lambda_i}\cos\left(2\pi(\nu_i t - \frac{x}{\lambda_i}\right) + \phi_i\right), \tag{4.10}$$

which we average over the width of the buoy by approximating

$$\sigma(t, x) \approx \frac{1}{3}\Big(\sigma\left(t, -\tfrac{1}{2}W\right) + \sigma(t, 0) + \sigma\left(t, \tfrac{1}{2}W\right)\Big). \tag{4.11}$$

The Lagrange equations for a wave of the form (4.9) are

$$\begin{aligned}
\frac{\mathrm{d}^2 z}{\mathrm{d}t^2} &= -g + \frac{g\rho_w S}{M}\Big(d + (Z_0 - z + A)\cos(\theta)\Big)\cos(\theta) - \gamma_z\frac{\mathrm{d}z}{\mathrm{d}t}, \\
\frac{\mathrm{d}^2\theta}{\mathrm{d}t^2} &= -\frac{g\rho_w S}{J}\Big(d + (Z_0 - z + A)\cos(\theta)\Big)(Z_0 - z + A)\sin(\theta) - \frac{k(\theta - \sigma)}{J} - \gamma_\theta\frac{\mathrm{d}\theta}{\mathrm{d}t},
\end{aligned} \tag{4.12}$$

where we have added friction terms with damping γ_z and γ_θ to take into account the friction due to water.

When there is no wave, no tilting of the buoy, and no friction, the equation governing the depth of the buoy is

$$\begin{aligned}
\frac{d^2 z}{dt^2} &= -g + \frac{g\rho_w S}{M}\left(\frac{L}{2} + (Z_0 - z)\right) \\
&= -\frac{g\rho_w S}{M}z.
\end{aligned} \tag{4.13}$$

Therefore, the bobbing frequency of the buoy is

$$\nu = \frac{1}{2\pi}\sqrt{\frac{g\rho_w S}{M}}. \tag{4.14}$$

We perform simulations for a hollow cylinder using the parameters listed in Table 1. With these parameters, the natural bobbing frequency for such a buoy is $\nu = 0.842$ Hz. If we excite the buoy with a monochromatic wave of frequency $\nu_\omega = 0.15$ Hz and wave length 10 m, so that the buoy bobs about and swings, then we observe the frequency spectrum for the vertical motion shown in Figure 6. When excited by a superposition of waves, similar to the one observed at sea (see Figure 3), we see, unsurprisingly, that the 3 frequencies appear in the spectrum, as shown in Figure 7. We notice that the rotational oscillations are excited at frequencies higher than the forcing frequencies, but not by a large amount.

Table 1. The parameters used for the buoy dynamics.

Parameter	Description	Value	Units
L	Height of the buoy	0.5	m
$r_b = W/2$	Radius of the buoy	0.5	m
ϵ	Thickness of the buoy	0.0194	m
k_w	Restoring "spring coefficient"	50	J
M	Mass of the buoy	275	kg
γ_z	Damping coefficient	0.3	s^{-1}
γ_θ	Damping coefficient	0.3	s^{-1}
J	Moment of inertia of the buoy	3.057	kg m^2

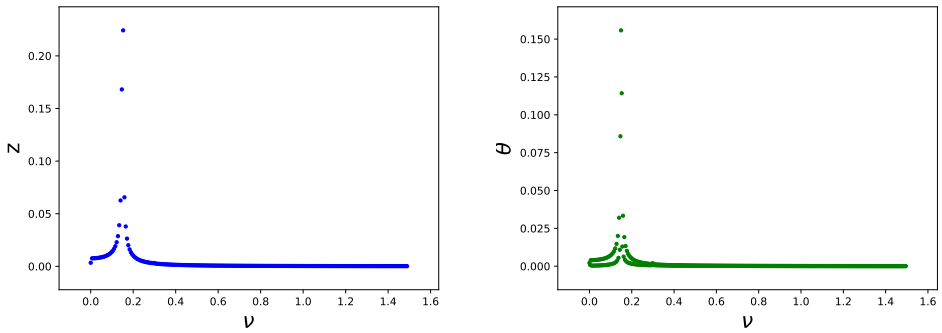

Figure 6. Vertical and rotational oscillation spectra for the buoy excited by a monochromatic wave of frequency $\nu = 0.15$ Hz.

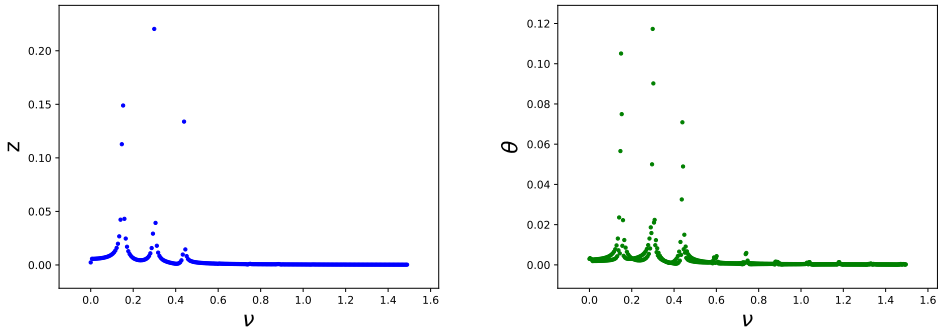

Figure 7. Vertical and rotational oscillations spectra for the buoy excited by a superposition of waves of frequencies 0.15 Hz, 0.3 Hz, and 0.44 Hz.

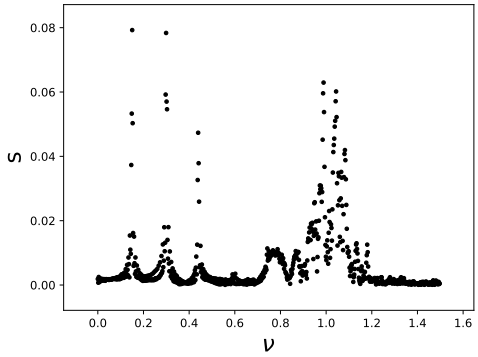

Figure 8. Horizontal spectrum of oscillation of the WITT with a cubic restoring force and excited by a superposition of waves of frequency 0.15 Hz, 0.3 Hz and 0.44 Hz. The spring constant is $k_b = 10^4$ m^{-2} s^{-2}.

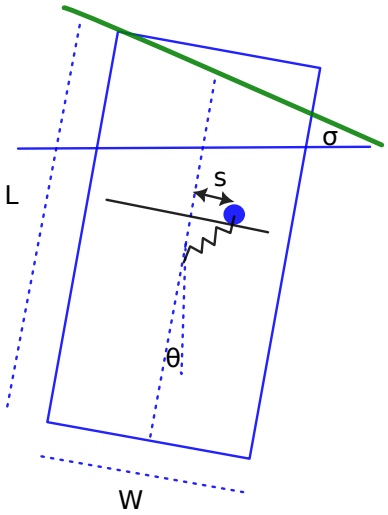

Figure 9. WITT on a sliding rail inside the buoy.

5 Perpendicular spring oscillator

To generate higher frequencies than the excitation frequency, one must use a nonlinear system. As a hypothetical case, if the WITT is attached to a spring with potential $V(s) = k_b s^4/4$, the equation governing the spring motion is then simply

$$\frac{\mathrm{d}^2 s}{\mathrm{d}t^2} = -k_b s^3. \tag{5.1}$$

As seen in Figure 8, this potential can excite frequencies higher than those of the forcing. The caveat is that the coefficient k_b must be very large. We now consider a physically realisable system that takes advantage of such nonlinearities.

One way to realise such a nonlinear oscillator is to constrain the WITT to move on a line or a plane, and attach it to a stiff spring which is at rest when the WITT is closest

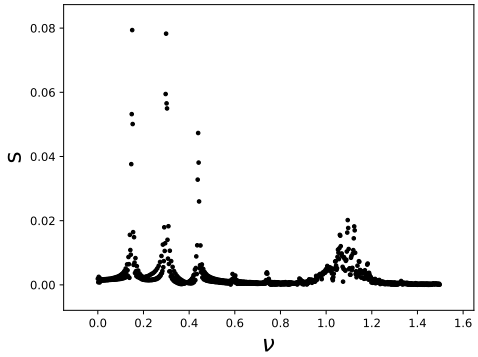

Figure 10. Horizontal spectrum of oscillation of the WITT on the horizontal rail in a buoy excited by a superposition of waves of frequency 0.15 Hz, 0.3 Hz and 0.44 Hz. The spring constant $k_b = 10^4$ m^{-2} s^{-2}.

to it as shown in Figure 9. The coordinates of the WITT on the buoy are

$$X = R\sin(\theta) + s\cos(\theta), \tag{5.2a}$$

$$Y = R\cos(\theta) - s\sin(\theta) + z, \tag{5.2b}$$

where z is the elevation of the buoy centre of mass, s is the distance along the plate, and θ is the angle the buoy makes with the vertical. The potential for this system is then

$$V = mgY + \frac{K}{2}\left(\sqrt{s^2+R^2} - R\right)^2, \tag{5.3}$$

where R is the length of the spring at rest, m is the mass of the WITT, and K is the spring constant. The Lagrangian is then

$$\mathcal{L} = \frac{m}{2}\left(\left(\frac{\mathrm{d}X}{\mathrm{d}t}\right)^2 + \left(\frac{\mathrm{d}Y}{\mathrm{d}t}\right)^2\right) - mgY - \frac{K}{2}\left(\sqrt{s^2+R^2} - R\right)^2. \tag{5.4}$$

The proper way to derive the equations of motion would be to add these to the Lagrangian of the buoy (given by (4.4), (4.5) and (4.8)), and derive equations for z, θ, and s. However, if the WITT is much lighter than the buoy, we can, as an approximation, derive the equation for s from the above Lagrangian and solve the new equation simultaneously with the buoy equations, using the values obtained from the buoy equations for θ, z, and their derivatives. The governing equation for s is then

$$\frac{\mathrm{d}^2 s}{\mathrm{d}t^2} = \frac{\mathrm{d}^2 z}{\mathrm{d}t^2}\sin(\theta) - R\frac{\mathrm{d}^2\theta}{\mathrm{d}t^2} + g\sin(\theta) + s\left(\frac{\mathrm{d}\theta}{\mathrm{d}t}\right)^2 - \frac{Ks}{m}\frac{\sqrt{s^2+R^2}-R}{\sqrt{s^2+R^2}}. \tag{5.5}$$

When we simulate the buoy movement in a wave made out of 3 components, we obtain the spectrum presented in Figure 10. We observe that there are indeed higher frequencies that the input frequencies. These will allow the WITT to harvest energy more effectively.

Another way to obtain this frequency amplification would be to have a buoy that is shaped in such a way that the floating restoring force does not vary linearly in z or θ, but varies as a power of z or θ. The design of such a buoy is a possible object of future study.

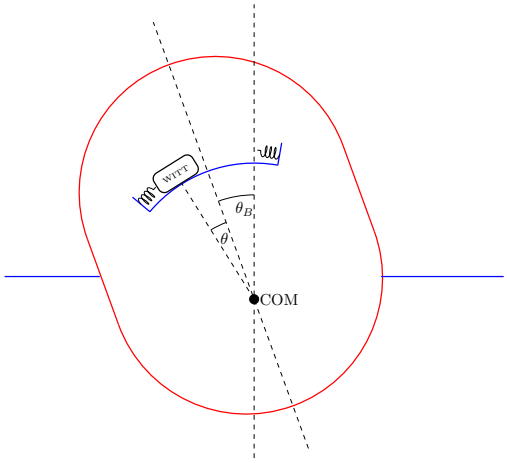

Figure 11. A simple diagram of the arc-rail concept.

6 Arched rail model

Another possible mechanism for how a nonlinear oscillator could be mounted inside a buoy is through an arched rail. The goal of the arched rail concept (which could also be implemented as an inverted pendulum) is to utilise energy from the slow oscillations of the wave to move the WITT along a rail, then stop its motion with a spring that will induce faster oscillations.

The WITT device is mounted to a convex rail mounted internally to the buoy with springs on either end to constrain it. As the buoy pitches, the device moves to one side. Then as the buoy pitches back, the arc of the rail keeps the device from moving until the rail is horizontal. After this point the device slides along the rail and impacts the other side. This impact kicks the pendulum within the device, generating electricity. The stiffness of the spring can be tuned to the device to get the desired frequency and cushion the impact. This storage and release of energy can be thought of as turning a simple, slow sinusoidal wave into one that is more square-like. The three-dimesional analogue of the arched rail would be a convex surface that the WITT moves around on, with springs around its perimeter.

Figure 11 shows a simple diagram of the concept. For simplicity, we assume that the centre of mass of the buoy is also the centre of the arc of the rail. The vertical motion of the buoy is ignored here, but is likely to have a positive effect on this concept. The friction of the device on the rail is modelled with a simple drag force. The parameters used are given in Table 2.

In this model, we need to solve for θ, the angle of the WITT device along the rail, and θ_B, the orientation of the buoy. The WITT is not in contact with the spring when $|\theta| < \theta_m$, and is in contact for angles larger than θ_m. The orientation of the buoy is assumed not to be influenced by the motion of the device and, is therefore, used as an input to the following system of equations based on the solution of the buoy model in

Table 2. The parameters used for the arched rail mechanism.

Parameter	Description	Value	Units
R	Radius of curvature of the rail	0.5	m
μ	Rail friction coefficient	0.1	N s m^{-1}
g	Strength of gravity	9.8	m s^{-2}
k	Spring stiffness	1000	N m^{-1}
D	Spring/WITT device damping	10	N s m^{-1}
θ_m	Half the angle used for the rail	0.07	rad

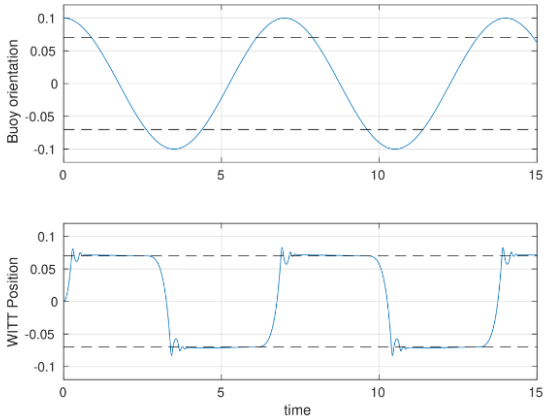

Figure 12. The buoy's orientation dictates when the device slides from one side to the other.

§4. When $|\theta| < \theta_m$,

$$\frac{\mathrm{d}^2\theta}{\mathrm{d}t^2} = \frac{1}{R}\Big(g\sin(\theta+\theta_B) - \mu\frac{\mathrm{d}\theta}{\mathrm{d}t}\Big), \tag{6.1}$$

while when $|\theta| \geq \theta_m$,

$$\frac{\mathrm{d}^2\theta}{\mathrm{d}t^2} = \frac{1}{R}\Big(g\sin(\theta+\theta_B) - k\big(\theta - \mathrm{sgn}(\theta)\,\theta_m\big) - D\frac{\mathrm{d}\theta}{\mathrm{d}t}\Big). \tag{6.2}$$

These equations are solved in MATLAB using the package `ifdiff` [15] to handle the system switching gracefully. As a first example, the system is tested with a regular sinusiodal forcing input. Figure 12 shows the mechanism building a store of gravitational potential energy and releasing it rapidly to generate higher frequencies.

Next, the output of the buoy mechanics simulation from §4 is used as an input. The results of this can be seen in Figure 13. The device switches sides less frequently and there is also a lot of motion in the buoy that does not influence the device's motion along the rail. It should be noted that the angles are taken in a reference frame rotating with the buoy, so the additional changes in orientation are also superimposed on the WITT's

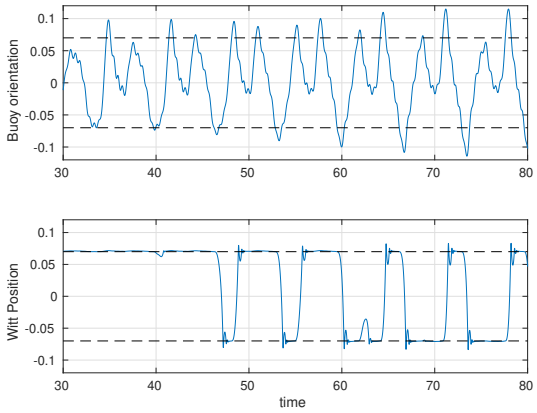

Figure 13. The buoy's orientation is much more irregular with more realistic waves, and the device does not switch sides in calm waters.

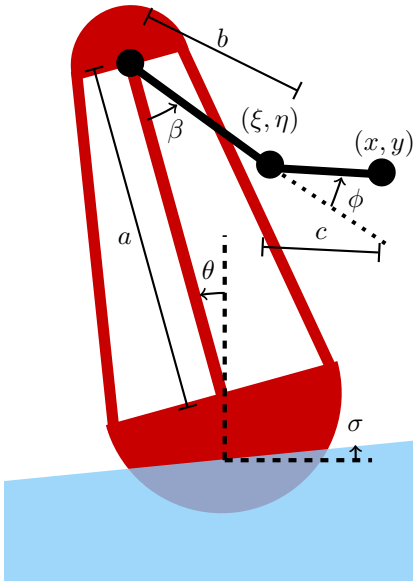

Figure 14. Geometry of the buoy and double pendulum.

orientation. The curvature of the rail imposes a minimum buoy orientation angle for which the device switches sides; this can be tuned depending how the buoy responds to the ocean conditions.

7 Pendulum model

A third possible nonlinear oscillator, which we model in this section, is a double pendulum attached to the top of a floating buoy. We envisage the WITT device attached to the end of a single pendulum inside the buoy, and the internal pendulum of the device is modelled as a second pendulum.

We show the geometry in Figure 14. We denote the height of the buoy by a, the length

of the first pendulum by b, and the length of the second pendulum by c. The fixed parts of the buoy are assumed to have moment of inertia J. The mass fixed to the first pendulum is denoted by M, and that fixed to the end of the second pendulum is m.

We have some freedom to chose a, b and J, subject to reasonable constraints on the size and weight of the buoy. The parameters c, M, and m are the pendulum length, fixed mass, and pendulum mass of the WITT, so are fixed by the WITT design.

To describe the motion, we let σ be the angle the surface of the water makes with the sea level, θ be the angle the buoy makes from vertical, β be the relative angle between the buoy and the first pendulum, and ϕ be the relative angle between the extension of the first pendulum and the second pendulum. We denote the position of first pendulum by (ξ, η), and that of the second pendulum by (x, y), as shown in Figure 14.

We begin by determining the position of the pendulums based on the angles. From this, we can determine the kinetic energy of the system and the potential energy of the masses. We also prescribe a potential to ensure the motion of the first pendulum is limited to ensure the system remains inside the buoy. Furthermore, we prescribe dissipative interactions. We then non-dimensionalise the system and numerically solve the associated Lagrange equations.

7.1 Model

We begin by expressing the position of the pendulums in terms of the angles θ, β, and ϕ. The position of the first pendulum is given by

$$\xi = -a\sin\theta + b\sin(\theta+\beta), \tag{7.1}$$

$$\eta = a\cos\theta - b\cos(\theta+\beta), \tag{7.2}$$

and the position of the second pendulum is given by

$$x = -a\sin\theta + b\sin(\theta+\beta) + c\sin(\theta+\beta+\phi), \tag{7.3}$$

$$y = a\cos\theta - b\cos(\theta+\beta) - c\cos(\theta+\beta+\phi). \tag{7.4}$$

The kinetic energy of the first mass is given by

$$T_1 = \frac{1}{2}M\left[\left(\frac{\mathrm{d}\xi}{\mathrm{d}t}\right)^2 + \left(\frac{\mathrm{d}\eta}{\mathrm{d}t}\right)^2\right], \tag{7.5}$$

and the kinetic energy of the second mass is given by

$$T_2 = \frac{1}{2}m\left[\left(\frac{\mathrm{d}x}{\mathrm{d}t}\right)^2 + \left(\frac{\mathrm{d}y}{\mathrm{d}t}\right)^2\right]. \tag{7.6}$$

We also consider the rotational kinetic energy of the buoy:

$$T_R = \frac{1}{2}J\left(\frac{\mathrm{d}\theta}{\mathrm{d}t}\right)^2, \tag{7.7}$$

where J is the moment of inertia. Thus, the total kinetic energy is given by

$$T = \frac{1}{2}M\left[\left(\frac{\mathrm{d}\xi}{\mathrm{d}t}\right)^2 + \left(\frac{\mathrm{d}\eta}{\mathrm{d}t}\right)^2\right] + \frac{1}{2}m\left[\left(\frac{\mathrm{d}x}{\mathrm{d}t}\right)^2 + \left(\frac{\mathrm{d}y}{\mathrm{d}t}\right)^2\right] + \frac{1}{2}J\left(\frac{\mathrm{d}\theta}{\mathrm{d}t}\right)^2. \tag{7.8}$$

Similarly, the potential energy of the two masses are

$$V_1 = Mg\eta, \quad V_2 = mgy. \tag{7.9}$$

We model the potential energy of the buoy as a harmonic oscillator with potential

$$V_R = k(\theta - \sigma)^2, \tag{7.10}$$

where k is the 'spring constant'. Recall the σ is the angle that the free-surface of the ocean makes to the horizontal. In this way, the buoy has a preference to be perpendicular to the surface of the water. Physically, the first pendulum's motion is constrained by the buoy. We therefore prescribe an additional potential $U(\beta)$ to impose this limit the range of β values. We assume this potential has the form

$$U(\beta) = E\left(\left(\frac{1}{\beta - \beta_{\max}}\right)^6 + \left(\frac{1}{\beta + \beta_{\max}}\right)^6\right), \tag{7.11}$$

where E is a scaling factor and $\beta_{\max}$ is the maximum allowable β (a more sophisticated model could use, for example, the so-called WCA potential traditionally used in molecular dynamics [17]). Therefore, the total potential energy of the system is

$$V = V_1 + V_2 + V_R + U(\beta) \tag{7.12}$$

$$= Mg\eta + mgy + k(\theta - \sigma)^2 + U(\beta). \tag{7.13}$$

We must also consider dissipative damping interactions. We assume the damping is of the form

$$R = \frac{1}{2}\gamma_\theta\left(\frac{\mathrm{d}\theta}{\mathrm{d}t} - \frac{\mathrm{d}\sigma}{\mathrm{d}t}\right)^2 + \frac{1}{2}\gamma_\beta(\beta)\left(\frac{\mathrm{d}\beta}{\mathrm{d}t}\right)^2 + \frac{1}{2}\gamma_\phi\left(\frac{\mathrm{d}\phi}{\mathrm{d}t}\right)^2, \tag{7.14}$$

where γ_θ, γ_β, and γ_ϕ are the associated damping coefficients of the buoy, first pendulum, and second pendulum, respectively. We assume that the damping coefficients for the buoy, γ_θ, and the second pendulum, γ_ϕ, are constant. However, due to the fact that the angle of the first pendulum, β, is limited, we take a more complicated damping term to reflect that there will be more dissipation when β approaches $\beta_{\max}$.

Firstly, suppose that the motion of the first pendulum is dominated by the potential $U(\beta)$, so then $\mathrm{d}^2\beta/\mathrm{d}t^2 \sim U'(\beta)$. Then, upon multiplying by $\mathrm{d}\beta/\mathrm{d}t$ and integrating with respect to t, we find

$$\frac{1}{2}\left(\frac{\mathrm{d}\beta}{\mathrm{d}t}\right)^2 \sim C_1 + U(\beta), \tag{7.15}$$

where C_1 denotes the energy of the system. Secondly, suppose that the motion of the first pendulum is dominated by a dissipation function, $f'(\beta)$. Then $\mathrm{d}^2\beta/\mathrm{d}t^2 \sim f'(\beta)\mathrm{d}\beta/\mathrm{d}t$. By integrating, we find

$$\frac{\mathrm{d}\beta}{\mathrm{d}t} \sim f(\beta) + B, \tag{7.16}$$

for a constant B. Equating these two expressions for $\mathrm{d}\beta/\mathrm{d}t$ from equations (7.15) and (7.16),

Table 3. Dimensional parameters for the pendulum model of §7.

Symbol	Description	Value
a	Height of buoy	1 m
b	Length of first pendulum	0.9 m
c	Length of second pendulum (internal WITT pendulum)	0.1 m
M	Mass of first pendulum (fixed parts of WITT device)	10 kg
m	Mass of second pendulum (internal WITT pendulum)	1 kg
J	Moment of inertia of the buoy	10 kg m^2
g	Acceleration due to gravity	10 m s^{-2}
k	'Spring constant' of buoy potential	100 N m^{-1}
E	Amplitude of theta potential	10^{-6} kg m^2 s^{-2}
$\beta_{\max}$	Maximum β value	0.3 rad
γ_θ	Damping coefficient of θ	30 kg m^2 s^{-1}
C	Damping coefficient of β	10 kg m^2 s^{-1}
γ_ϕ	Damping coefficient of ϕ	3×10^{-4} kg m^2 s^{-1}
A	Amplitude of σ oscillations	0.3 rad
ω	Wave driving frequency	$2\pi \cdot 0.3$ s^{-1}

we find $U(\beta) \sim f(\beta)^2$, so we take the dissipation, $\gamma_\beta(\beta) = f'(\beta)$, to be of the form

$$\gamma_\beta(\beta) = C \left| \frac{U'(\beta)}{\sqrt{U(\beta)}} \right|, \tag{7.17}$$

where C is a constant and $U(\beta)$ is given by (7.11).

Finally, for simplicity we assume the angle of the water σ follows the sinusoid

$$\sigma(t) = A \sin(\omega t), \tag{7.18}$$

where A is the amplitude and ω is the angular frequency of the waves. The parameters are summarised in Table 3. We now transition to the non-dimensionalisation of our problem.

7.2 Non-dimensionalisation

We scale the position coordinates with the length of the buoy, a, and time with the reciprocal of the frequency of the prescribed forcing, ω. Using hats to denote dimensionless variables, we have

$$\xi = a\hat{\xi}, \quad \eta = a\hat{\eta}, \quad x = a\hat{x}, \quad y = a\hat{y}, \quad t = \frac{1}{\omega}\hat{t}. \tag{7.19}$$

Upon scaling the kinetic and potential energy with the kinetic energy of the WITT

device, $(T, V) = Ma^2\omega^2(\hat{T}, \hat{V})$, we find

$$\hat{T} = \frac{1}{2}\left[\left(\frac{\mathrm{d}\hat{\xi}}{\mathrm{d}\hat{t}}\right)^2 + \left(\frac{\mathrm{d}\hat{\eta}}{\mathrm{d}\hat{t}}\right)^2\right] + \frac{1}{2}m_1\left[\left(\frac{\mathrm{d}\hat{x}}{\mathrm{d}\hat{t}}\right)^2 + \left(\frac{\mathrm{d}\hat{y}}{\mathrm{d}\hat{t}}\right)^2\right] + \frac{1}{2}J_1\left(\frac{\mathrm{d}\theta}{\mathrm{d}\hat{t}}\right)^2, \tag{7.20}$$

$$\hat{V} = g_1\hat{\eta} + m_1 g_1\hat{y} + k_1(\theta - \sigma) + E_1\left(\frac{1}{(\beta - \beta_{\max})^6} + \frac{1}{(\beta + \beta_{\max})^6}\right), \tag{7.21}$$

where the parameters are:

$$m_1 = \frac{m}{M}, \quad J_1 = \frac{J}{Ma^2}, \quad g_1 = \frac{g}{a\omega^2}, \quad k_1 = \frac{k}{Ma^2\omega^2}, \quad E_1 = \frac{E}{Ma^2\omega^2}. \tag{7.22}$$

Here, m_1 is the mass ratio between the mass within the WITT to the WITT device, J_1 is the ratio of the moment of inertia of the buoy to that of the first pendulum, g_1 is the ratio of gravity to the natural acceleration scale, and k_1 and E_1 are k and E scaled by the natural energy scale of the system, respectively. We scale the dissipation with $R = Ma^2\omega^3\hat{R}$, then in dimensionless form, (7.14) reads

$$\hat{R} = \frac{1}{2}\gamma_{\theta 1}\left(\frac{\mathrm{d}\theta}{\mathrm{d}\hat{t}} - \frac{\mathrm{d}\sigma}{\mathrm{d}\hat{t}}\right)^2 + \frac{1}{2}\gamma_{\beta 1}\left|\frac{\hat{U}'(\beta)}{\sqrt{\hat{U}(\beta)}}\right|\left(\frac{\mathrm{d}\beta}{\mathrm{d}\hat{t}}\right)^2 + \frac{1}{2}\gamma_{\phi 1}\left(\frac{\mathrm{d}\phi}{\mathrm{d}\hat{t}}\right)^2, \tag{7.23}$$

where $\hat{U}(\beta)$ is the dimensionless potential for β, and we have introduced the parameters

$$\gamma_{\theta 1} = \frac{\gamma_\theta}{Ma^2\omega}, \quad \gamma_{\beta 1} = \frac{C}{Ma^2\omega}, \quad \gamma_{\phi 1} = \frac{\gamma_\phi}{Ma^2\omega}. \tag{7.24}$$

We now construct the Lagrangian, $\mathcal{L} = T - V$, of the system. The non-conservative frictional damping of the pendulums are included via the dissipation function, R. Using the Euler–Lagrange equations along with Rayleigh's dissipation function [14] gives the governing equations

$$\frac{\mathrm{d}}{\mathrm{d}\hat{t}}\left(\frac{\partial\mathcal{L}}{\partial\theta'}\right) - \frac{\partial\mathcal{L}}{\partial\theta} + \frac{\partial R}{\partial\theta'} = 0, \tag{7.25a}$$

$$\frac{\mathrm{d}}{\mathrm{d}\hat{t}}\left(\frac{\partial\mathcal{L}}{\partial\beta'}\right) - \frac{\partial\mathcal{L}}{\partial\beta} + \frac{\partial R}{\partial\beta'} = 0, \tag{7.25b}$$

$$\frac{\mathrm{d}}{\mathrm{d}\hat{t}}\left(\frac{\partial\mathcal{L}}{\partial\phi'}\right) - \frac{\partial\mathcal{L}}{\partial\phi} + \frac{\partial R}{\partial\phi'} = 0, \tag{7.25c}$$

where the prime denotes differentiation with respect to $\hat{t}$. These equations are supplemented with initial conditions for the angle and the velocity of the angle. We assume that initially all pendulums are at rest in their equilibrium positions, so take the initial conditions to be

$$\theta = \beta = \phi = \frac{\mathrm{d}\theta}{\mathrm{d}\hat{t}} = \frac{\mathrm{d}\beta}{\mathrm{d}\hat{t}} = \frac{\mathrm{d}\phi}{\mathrm{d}\hat{t}} = 0 \quad \text{at } t = 0. \tag{7.26}$$

7.3 Numerical Simulation

We now solve the system of three ODEs (7.25) numerically, subject to initial conditions (7.26) and wave forcing given by (7.18), using Mathematica's `NDSolve`. The di-

Table 4. Dimensionless parameters for the pendulum model of §7.

Symbol	Definition	Description	Typical value
m_1	m/M	Pendulum mass ratio	0.1
J_1	J/Ma^2	Moment of inertia mass ratio	1
g_1	$g/a\omega^2$	Normalised gravitational acceleration	2.8
k_1	$k/Ma^2\omega^2$	Normalised spring constant	2.8
E_1	$E/Ma^2\omega^2$	Normalised potential strength	2.8×10^{-8}
γ_{θ_1}	$\gamma_\theta/Ma^2\omega$	Normalised damping coefficient of θ	1.6
γ_{β_1}	$C/Ma^2\omega$	Normalised damping coefficient of β	0.53
γ_{ϕ_1}	$\gamma_\phi/Ma^2\omega$	Normalised damping coefficient of ϕ	1.6×10^{-5}

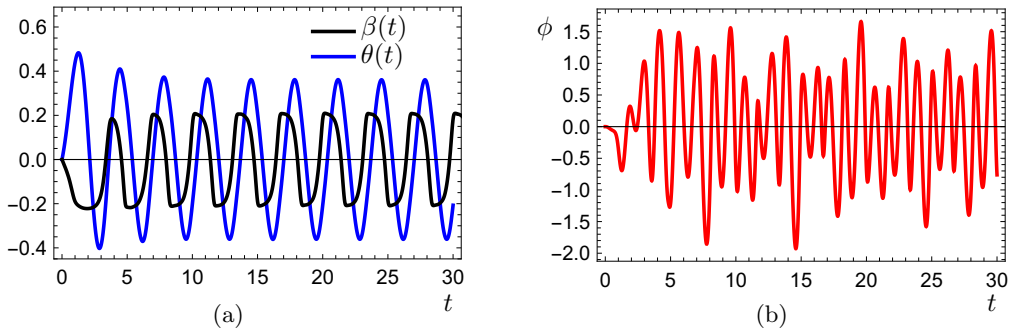

Figure 15. Angle of the buoy and two pendulums plotted against time, with the parameter values used given in Table 3. The forcing waves are of the form (7.18).

mensional parameter values used are given in Table 3, with corresponding dimensionless parameters given in Table 4. We see in Figure 15a that the buoy and first pendulum oscillate at approximately the same frequency, though the range of β is constrained by the imposed potential (7.14). To effectively harvest energy, it is the pendulum inside the WITT that needs to oscillate at a higher frequency, and we see from Figure 15b that it is indeed the case that ϕ oscillates more rapidly than the buoy or WITT device itself. So, even with the input, σ, being below the ideal frequency for the WITT, this double pendulum setup inside the buoy can allow energy to be harvested more effectively than if it were simply placed inside the buoy.

Next, we utilise the work done in §4 by using the buoy data to prescribe θ directly. This will give more realistic results as it directly uses wave data as an input. As the dynamics for $\theta(t)$ are given, we therefore only need to solve for the angles of the the two pendulums, β and ϕ. The governing equations are given by (7.25b) and (7.25c), and as initial conditions we again prescribe the pendulums to be at rest at their equilibrium positions.

In Figure 16 we see how the angles of the pendulums vary with time. We observe that despite there being some higher frequency modes in the buoy movement, the first pendulum oscillates at a relatively low frequency of approximately 0.3 Hz, which is lower than the 1.2 Hz required to effectively harvest energy from the WITT device. However,

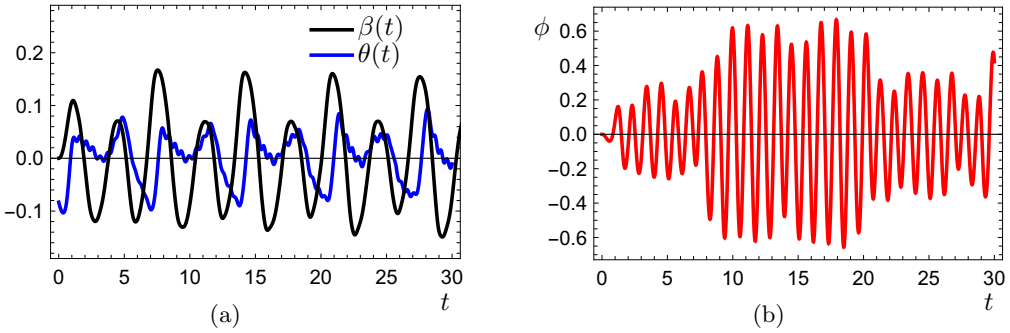

Figure 16. A plot of the angle of the two pendulums plotted against time, where θ is prescribed from the buoy motion calculations in §4. The parameter values used given in Table 3.

the second pendulum oscillates more rapidly, at about 1 Hz. Although lower than the 1.2 Hz that is aimed for, is substantially higher than the input frequency.

These simulations have shown that having a double pendulum inside a buoy gives the possibility of increasing the frequency that the WITT device oscillates. The physical parameters used in these simulations are just estimates, and so changing them could give rise to higher frequency oscillations, as discussed in the following subsection. One aspect of the WITT device that has not been considered in this double pendulum example is the power generation from the WITT itself. This generation is linked with the damping coefficient to the second pendulum, and so while having a lower damping coefficient can potentially increase the frequency of oscillation of the second pendulum, more work is needed to understand the amount of damping needed for optimal power production.

7.4 Optimisation for pendulum model parameters

From Figure 16, we observe slow oscillations of the buoy and first pendulum in Figure 16a, but fast oscillations of the second pendulum in Figure 16b. To understand which parameters from the model cause the fast oscillations in $\phi(t)$, we employ optimisation on the parameters of the governing equations (7.25), where we define an objective function that captures the contribution of high-frequency components to the oscillations in $\phi(t)$. We use the discrete Fourier transform to identify these components. The objective function is the sum of the squares of the high-frequency components (> 1.2 Hz) of the Fourier transform of $\phi(t)$. By maximising this objective function using the Nelder–Mead optimisation method [13], we identify the parameter values that maximise the fast oscillations in $\phi(t)$ and potentially increase the amplitude of high-frequency oscillations. In this context, "high-frequency oscillations" refer to the oscillations that occur at frequencies higher than the specified threshold of 1.2 Hz and "amplitude" refers to the magnitude of these oscillations.

The optimisation approach begins with an initial guess for the varying parameters, we vary the dimensionless spring constant, k_1, damping coefficients, γ_{β_1} and γ_{ϕ_1}, and driving frequency, ω. The driving frequency is determined by the wave frequency hitting the device and while this may be externally controlled or influenced by natural wave conditions, understanding its impact is crucial. This understanding is typically achieved

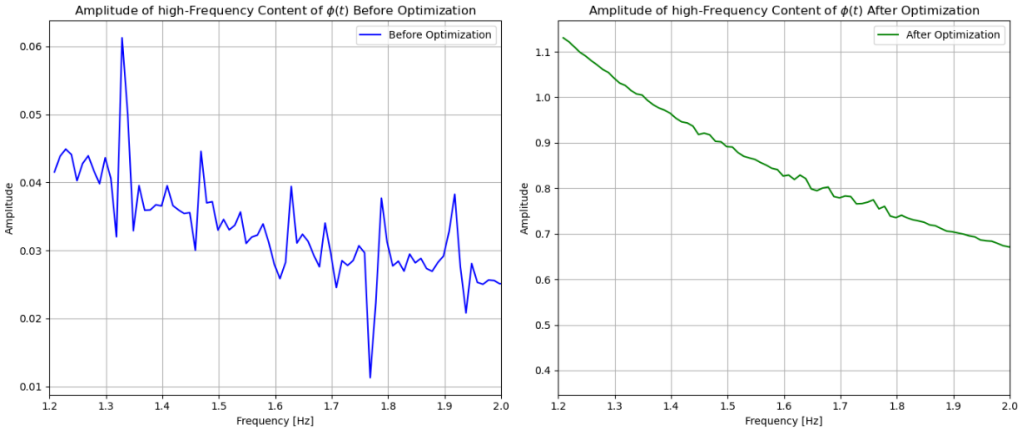

Figure 17. Amplitude of frequency content of $\phi(t)$ before (left) and after (right) optimisation, showing a significant increase in high-amplitude frequencies.

through sensitivity analysis, which identifies the most influential parameters that could be done as a future work and then optimization fine-tunes these parameters to improve system performance. Even if ω is not directly controllable, understanding its role can inform design adjustments (for example, using a nonuniform buoy that effectively amplifies the driving frequency) or operational strategies to match typical wave conditions. Optimising for ω also gives insight into how effective the pendulum mechanism will be across different use cases of the WITT (i.e. different ocean and weather conditions).

The system of governing differential equations (7.25) is solved in python by using the 'RK45' method [9] for each iteration. The discrete Fourier transform of $\phi(t)$ is then computed to analyse its frequency components and then the objective function is evaluated for the solution. By iteratively adjusting the parameters to maximise the objective function, the optimisation process identifies the parameter values that increase high-frequency oscillations in $\phi(t)$.

The results of this optimisation are illustrated in Figure 17. As we are interested in high-frequency oscillations, we focus on frequencies between 1.2 Hz and 2.0 Hz. The left plot shows the frequency content and its amplitude of $\phi(t)$ before optimisation, using parameters given in Table 4, where the frequencies of interest exhibit amplitudes between 0.01 and 0.06. On the other hand, the right plot shows the results after optimisation, where we see significant increase in amplitudes to the range of 0.6 to 1.1. This increase shows the effectiveness of the optimisation process in maximising the high-frequency oscillations. This indicates that the optimisation not only ensured that the oscillations occurred at the desired higher frequencies (1.2 Hz) but also increased the magnitude of these oscillations, making them stronger and more effective for energy harvesting purposes.

The optimisation adjusted the spring constant, k_1, damping coefficients, γ_{β_1} and γ_{ϕ_1}, and driving frequency, ω, to achieve the outcome. Using our experimental data, the optimised parameters were $k_1 = 2.93$, $\gamma_{\beta_1} = 5.40$, $\gamma_{\beta_1} = 1.51 \times 10^{-5}$, and $\omega = 1.90$, indicating that increasing the spring constant and the damping coefficient for γ_{β_1}, while

significantly reducing the damping coefficient for γ_{ϕ_1} is crucial in maximising the high-frequency oscillations. We also find, as expected, that a high driving frequency maximises these high-frequency oscillations, highlighting the importance of e.g. buoy design and other mechanisms that may be combined with the pendulum to increase ω. Increasing the damping coefficient γ_{β_1} stabilizes the low-frequency oscillations induced by the ocean waves, reducing low-frequency interference. These low-frequency oscillations, if left undamped, could create disturbances that interfere with the second pendulum's high-frequency oscillations. As a result, the overall system can achieve more stable and focused high-frequency oscillations, enabling the WITT device to harvest energy more effectively. The optimized driving frequency is $\omega = 1.90 \approx 2\pi \times 0.3$, so the input waves are of the frequency observed in the ocean wave data [8], reinforcing that this approach could lead to the necessary high-frequency oscillations.

While not performed in this study, a detailed sensitivity analysis of the optimised parameters would also be valuable for understanding the robustness of the design. Such an analysis would involve systematically varying each parameter within a certain range and observing the effects on the system's performance. By quantifying how sensitive the high-frequency oscillations are to changes in parameters like the spring constant, damping coefficients, and driving frequency, we can identify which parameters are most critical to maintain within tight tolerances. This information is essential for ensuring the reliability and efficiency of the WITT device under different operating conditions and in the presence of uncertainties [4, 5]. Finally, investigating the power generation capabilities of the WITT device in more detail, particularly the relationship between the damping coefficient and power production, is essential for optimising overall energy harvesting efficiency. These future research and development efforts will be critical in fully realising the capabilities of the WITT device and contributing to sustainable energy solutions.

8 Discussion and future work

One general difficulty with this project is that it is difficult to write down a set of equations that describe the motion of the buoy and an internal mechanism. In the course of the study group, most of the models that we produced were one- or two-dimensional, since producing more complex models with potentially non-uniform geometry was beyond the scope of the week. However, we hope the models we have produced provide suitable proofs of concepts and idea generation based upon which more detailed computational and experimental studies can be undertaken. There is also a vast array of potential ideas for how the device could be mounted to the buoy.

There were some challenges that we did not address in the week. Firstly, we did not address the design of the buoy. During the study group we assumed the buoy to have a uniform cylindrical shape for mathematical convenience. In a real-world deployed system, it may be possible to design a buoy in such a way that it accentuates the type of motion required by the WITT device. Using a buoy that is non-uniform in shape, it may be possible to create nonlinear effects that enhance the oscillations of the buoy as it is driven by the ocean. However, designing such a buoy may require simulation of the whole system using computational fluid dynamics and input by experts in marine engineering.

During the study group, it was also suggested that it may be possible to have a buoy

that is filled with fluid, which sloshes as the buoy oscillates, adding to the instability of the buoy. How this phenomena, known as the 'free-surface effect' [10], could be incorporated into the design of a purposely unstable buoy, and whether it could prove impactful at the scale of the buoy, is unknown to the authors, but could be a potential avenue of future work. It may also be possible to design a buoy, which, similarly to the arced rail setup, generates nonlinear effects by using the low frequency oscillations driven by the ocean to build a store of potential energy, which is then rapidly released and converted into higher frequency oscillations that can be harvested by the WITT as power.

There is also the open question of how other objects could be coupled to the buoy. Obviously, the buoy will require some system to stop it drifting away from its deployment. This is traditionally done by tethering the buoy to an anchor point. Hence, it could be of interest to model how the tethering system interacts with the buoy, and whether a tether can be designed in such a way that it augments the motion of the buoy, or even generates the high frequency oscillations needed to effectively generate power. Other features could be added to the buoy, such as sails to generate additional rotation, or devices to make the buoy more stable if required, such as fins or outriggers. It may also be possible to couple buoys together, so that there are interactions between their motion that may be useful for power generation.

Since the goal of the device is to generate electrical power, we did not consider systems that require electricity to function. However, it can be imagined that a buoy could be designed that also charges a very small electrical system, that could respond to sea or wind conditions or act in an emergency to move the system from an unfavourable position, for example, being stuck on one side unable to be righted. However, this may not be advisable, as the device should be small enough to power the sensors that it is connected to and is not expected to generate large amounts of other power.

Potential extensions of this work may require input from a variety of specialists. In particular, a simulation of the fluid mechanics of the buoy and surrounding waves, giving insight into how the device interacts with various sea states may be needed. There may need to be optimisation of the parameters and properties of the buoy and device mounting in order to have the best response to the expected sea conditions where it will be deployed. Also, there remains the open question of how best to set up a system that has the nonlinear behaviour we require, such as a cubic restoring force, and if there is a mechanically simple and low-maintenance way to do this at the required scale.

9 Executive summary

During the study group we have explored the design of a wave energy converter based on the WITT, a device that converts motion and rotation in all six degrees of freedom into electrical power. The principle behind the wave energy converter is to attach the WITT to a buoy in such a way that the WITT is able to generate power from the motion of the buoy due to incoming waves. The present difficulty in deploying such a device effectively is that the typical frequencies of ocean waves are an order of magnitude lower than the frequency of oscillation required for the WITT to function optimally.

Our challenge is therefore to design a buoy, including the WITT, that will naturally respond to low-frequency ocean waves by bobbing or otherwise oscillating the WITT at a

higher frequency. Based on mathematical and physical reasoning, we posit that this effect cannot be achieved through the bobbing motion of a uniformly-shaped buoy, nor through a linear mechanism (for example, a simple spring or pendulum) within the buoy, as any such mechanism will only reproduce the oscillation imposed by the ocean. Instead, we infer that nonlinear dynamics are required to produce the desired motion of the WITT, and explore several means that such dynamics may be achieved, taking the canonical example of the Duffing oscillator as motivation.

We begin by writing and solving a mathematical model for a cylindrical buoy that bobs and rolls in response to an idealised model of ocean waves. It may be possible to achieve nonlinear bobbing dynamics and high-frequency oscillation by designing a buoy that is not uniformly shaped. However, we deemed the problem of designing, simulating, and optimising such a buoy to be beyond the scope of the study group, as such an investigation would likely require advanced computational physics software and/or additional expertise, for example, of marine engineers. Instead, we focused on possible mechanisms for mounting the WITT within the buoy, upon which the buoy motion found above can be imposed during simulation.

We first explore a perpendicular spring oscillator, following the original setup of the Duffing oscillator, where the WITT is constrained to move horizontally relative to the buoy and attached to a fixed spring. By modelling and simulating this setup, we show that the desired high-frequency response can be achieved. However, a very stiff spring is required to elicit this response.

Second, we consider a setup where the WITT device moves on an arched rail within the buoy, and collides with a spring at either end of the rail. As the buoy tips in response to waves, the WITT slides from one end of the rail to the other and bounces rapidly on the opposite spring, producing the high-frequency oscillation required once more. Again, a simulation confirms that such a device is able to produce the required oscillation frequencies in principle.

Third, we consider mounting the WITT on a double pendulum attached to a buoy with the upper pendulum bound between two walls. Once more, we show as before that such a setup is able to produce the desired results, and consider in addition how features of such a design, such as pendulum length or relative mass, may be chosen to optimise the frequency enhancement.

In conclusion, we have therefore obtained proof of concept for several mechanisms that a WITT device within a buoy could effectively harness wave energy. With this said, additional research and expert insight is required to determine how feasible these designs are to implement in a way that is low-maintenance and scalable. Factors such as size, cost, and durability of the buoy device must be taken into consideration. We also note that there are many possible ways to achieve nonlinear dynamics that are beyond the scope of our consideration, such as through non-uniform buoy design, mechanisms based on the free-surface effect, a tethering system, or an electrical device within the buoy. The continuation of the ideas presented in this report and the exploration of those that have proved beyond our scope therefore present many promising avenues for future research.

10 Key recommendations

Based on our work completed during the study group and summarised in the above report, we make the following recommendations:

- Future research aimed at designing a buoy to convert wave energy via the WITT should focus on achieving nonlinear dynamics. Such research may explore any of a broad range of possible mechanisms or designs.
- Further research is required into designing and optimising a non-uniform buoy, in order to achieve a nonlinear dynamical response to wave motion.
- Insight from marine engineers and computational physics software is required to better understand the complex problem of nonuniform buoy motion.
- Mechanisms such as a perpendicular spring, arched rail, double pendulum, or adaptations of these pendulums, have the potential to provide the required frequency enhancement for the WITT to function as a wave energy converter. Further research is required to determine the optimal design for such devices, and whether such a design is practical and cost-effective to implement physically. This will require a combination of mathematical modelling and engineering insight.

Acknowledgements

The authors of this report acknowledge support from ESGI 180 hosts and sponsors: International Centre for Mathematical Sciences; UK Knowledge Exchange Hub for Mathematical Sciences; College of Engineering and Physical Sciences, University of Birmingham; School of Mathematics, University of Birmingham; Business Engagement and Research Impact (BERI) team, University of Birmingham; and the Mathematics in Medical and Life Sciences journal. We also thank our industrial partners Mairi and Martin Wickett for helpful discussions.

References

[1] P.S. Addison. *Fractals and Chaos: An illustrated course*. CRC Press, 1997.

[2] C. Anning. Modelling the WITT device suspended between two springs: A mathematical approach. Master's thesis, Department of Engineering Mathematics, University of Bristol, 2023.

[3] E. Butler, Y. Darbar, P. Kaklamanos, A. Lacey, E. Luckins, P. Morawiecki, N. Nguyen, E. Peroni, C. Please, J. Roberts, C. Spalding, R. Whittaker, H. Xu, and M. Zyskin. "Whatever Input to Torsion Transfer": Harvesting energy from a WITT gearbox device. In *Proceedings of the 167th European Study Group with Industry*, 2022.

[4] Q. Cai and S. Zhu. Nonlinear double-mass pendulum for vibration-based energy harvesting. *Nonlinear Dyn*, 112:5109–5128, 2024.

[5] J. Chen, B. Bao, J. Liu, Y. Wu, and Q. Wang. Pendulum energy harvesters: A review. *Energies*, 15(22):8674, 2022.

[6] S. Crowley, R. Porter, D. J. Taunton, and P. A. Wilson. Modelling of the WITT wave energy converter. *Renewable energy*, 115:159–174, 2018.

[7] G. Duffing. *Erzwungene Schwingungen bei veränderlicher Eigenfrequenz und ihre technische Bedeutung*. Number 41–42. Vieweg, 1918.

[8] WITT Energy, 2023. Private communication.

[9] Erwin Fehlberg. *Low-order classical Runge–Kutta formulas with stepsize control and their application to some heat transfer problems*. National aeronautics and space administration, 1969.

[10] J. B. Frandsen. Sloshing motions in excited tanks. *Journal of computational physics*, 196(1):53–87, 2004.

[11] P. Jordan, D. W.; Smith. *Nonlinear ordinary differential equations – An introduction for scientists and engineers*. Oxford University Press, 4th edition, 2007.

[12] H. Lamb. *Hydrodynamics*. Camb. Univ. Press, 1895.

[13] J. A. Nelder and R. Mead. A simplex method for function minimization. *The Computer Journal*, 7:308–313, 1965.

[14] Lord Rayleigh. The Dissipation Function. In *The Theory of Sound*, pages 78–79. MacMillan Co., London, 1877.

[15] A. Sommer, K. Folger, and M. Strik. ifdiff - a MATLAB toolkit for ODEs with state-dependent switches, *https://github.com/andreassommer/ifdiff*, Visited on 26/6/2024.

[16] T. Watts. Exploring feasible deployment solutions for a novel marine renewable energy device. Master's thesis, Department of Engineering Mathematics, University of Bristol, 2023.

[17] J. D. Weeks, D. Chandler, and H. C. Andersen. Role of repulsive forces in determining the equilibrium structure of simple liquids. *The Journal of Chemical Physics*, 54(12):5237–5247, 1971.